PHYSICAL REVIEW C VOLUME 46, NUMBER 5 NOVEMBER 1992

Systematics of inclusive pion double charge exchange in the delta resonance region

S. A. Wood,* J. L. Matthews, and E. R. Kinney†
Department of Physics and Laboratory for Nuclear Science, Massachusetts Institute of Technology, Cambridge, Massachusetts 02139

P. A. M. Gram
Los Alamos National Laboratory, Los Alamos, New Mexico 87545

G. A. Rebka, Jr. and D. A. Roberts‡
Department of Physics, University of Wyoming, Laramie, Wyoming 82071

(Received 21 February 1992)

A systematic study of inclusive pion double charge exchange is reported for nuclei between $A=16$ and $A=208$. The doubly differential cross sections for the $A(\pi^+,\pi^-)$ and $A(\pi^-,\pi^+)$ reactions in ^{16}O, ^{40}Ca, ^{103}Rh, and ^{208}Pb were measured at incident energies between 120 and 270 MeV at three to five outgoing pion angles. Pion spectra were measured over the energy range from 10 MeV to the kinematic limit for double charge exchange. Integrating these spectra over outgoing pion energy generated angular distributions, and subsequently integrating these angular distributions generated total reaction cross sections. The shapes of the measured spectra are compared with those determined by the distribution of events in four-body phase space and with those predicted by a model in which the pion undergoes two sequential single charge exchanges on nucleons in a Fermi gas. The cross sections are compared with predictions of cascade calculations in which more than two interactions, including pion absorption and scattering without charge exchange, may occur.

PACS number(s): 25.80.Gn, 25.80.Hp, 25.80.Ls

I. INTRODUCTION

Pion double charge exchange (DCX) provides a direct means of investigating multiple pion interactions in nuclei. Although all pion-nucleus reactions involve multiple interactions between pions and nucleons to some degree, pion double charge exchange requires the participation of at least two like nucleons whose charges are changed in the process. The participating nucleons are not free, and little is known of the intermediate state of the nucleus during the reaction before the rearrangements necessary to conserve charge and to emit a single oppositely charged pion are accomplished. A systematic investigation of inclusive DCX, for which the final arrangement of nucleons is unspecified, has been undertaken in a wide range of nuclei to gain insight into the mechanisms of multiple pion-nucleon scattering.

DCX reactions leading to discrete final nuclear states have received considerable attention since 1977, but prior to the experiments reported here, observation of the inclusive reaction has been limited. A few measurements of DCX in ^{3}He [1] and ^{4}He [2–4] were performed whose major objective was to satisfy persistent curiosity about the existence of trineutron and tetraneutron states in the continuum. None have been found [5]. Owing to the faint beams, serious backgrounds, and small cross sections that they encountered, these pioneering experiments produced only a few complete momentum spectra at isolated incident energies and angles of observation. The earliest measurements [6] on complex nuclei used emulsions with the attendant difficulties. In 1964–1965, Gilly *et al.* [3,7] used a simple spectrometer to measure, at 0°, the excitation functions of double charge exchange initiated by negative pions in He, Be, Li, and C. Unfortunately, these excitation functions do not lend themselves to estimation of the cross sections or to a discussion of the systematics of the reaction. The same equipment was used to acquire partial momentum spectra with very limited statistics from (π^+,π^-) reactions in Li, Be, and Na.

The first experiment with good coverage of outgoing pion energies and angles was the measurement in 1980 of the cross section for the ^{16}O$(\pi^+,\pi^-)X$ process at 240 MeV performed at the Swiss Institute for Nuclear Research [now the Paul Scherrer Institute (PSI)] [8]. Doubly differential cross sections were measured with good statistical accuracy for outgoing pion energies between 35 and about 200 MeV at 50°, 85°, and 130°.

A simple model in which DCX occurs by two successive single charge exchange processes is depicted in Fig. 1(a). We have illustrated the process for ^{4}He, but any nucleus with two or more neutrons would support the (π^+,π^-) reaction just as any nucleus with two or more protons would support the (π^-,π^+) reaction. In fact, most of the previous theoretical calculations of DCX have been specific to ^{3}He [9–13] and ^{4}He [12–18]; their

---

*Present address: Continuous Beam Electron Accelerator Facility, Newport News, VA 23606.

†Present address: Department of Physics, University of Colorado, Boulder, CO 80309.

‡Present address: Department of Physics, University of Michigan, Ann Arbor, MI 48109.

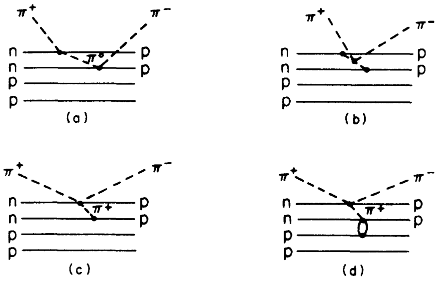

FIG. 1. Possible reaction mechanisms for inclusive double charge exchange. (a) Sequential single charge exchange. (b) Scattering from exchange pion. (C) Off-shell pion production followed by absorption of extra pion on a nucleon. (d) Pion production followed by absorption of extra pion on a nucleon pair.

extension to heavier nuclei is not clear. Moreover, calculations based on the mechanism illustrated in Fig. 1(a) [11,18] and on the alternative mechanisms illustrated in Figs. 1(b) [15], and 1(c) and 1(d) [19] have not achieved quantitative success in reproducing the available data [1,3,4,19–23].

Until recently, the theoretical literature on DCX in heavier nuclei was very sparse [24–26]. Batusov, Kochkin, and Mal'tsev [25] performed a classical cascade calculation and compared the results with the emulsion data. They found fairly good agreement with the measured energy spectra, but not with the observed angular distributions. Hüfner and Thies [26] used a simple and elegant approach based on the Boltzmann equation to describe the propagation and scattering of pions in a nucleus. This model qualitatively reproduces many of the features of pion absorption and scattering, and predicts that the total DCX cross section in ^{12}C rises rapidly with energy, peaking at ~225 MeV, well above the Δ-resonance energy. Another interesting prediction of this model is the relative importance of triple scattering in the various pion reaction channels. Although insignificant in other channels, triple scattering can be shown [27] to account for approximately one-third of the DCX cross section in ^{16}O at 240 MeV.

In the last few years, Oset and co-workers [28–30] have embarked on an ambitious program to calculate the total cross sections for all of the inclusive pion-nucleus reaction channels simultaneously, in the framework of a Δ-hole model, i.e., the excitation of a nucleon into a Δ isobar, leaving a nucleon hole state in the residual nucleus, and the subsequent propagation of this excited nuclear state. In the calculations of Oset and co-workers, the intrinsic probability of each reaction is evaluated in infinite nuclear matter using many-body techniques; the probabilities are calculated for finite nuclei through a local density approximation. The cross sections are then estimated by a cascade-style Monte Carlo method in which pions and nucleons propagate as classical particles between interactions. Pions are followed until they escape, not necessarily with their original charge, or are absorbed. Predictions of this model have been compared [29,30] with some of the results of the present experiment [27,31].

Because theoretical analysis of pion multiple scattering is difficult, systematic observation of DCX in several nuclei and over an extensive range of kinematic variables is an important step toward identifying the essential features of the reaction. We present here a study, carried out at the Clinton P. Anderson Meson Physics Facility (LAMPF), designed to yield accurate measurements of absolute doubly differential cross sections for the DCX reaction in a series of nuclei from $A=16$ to 208. The most nearly complete data were obtained for the (π^+,π^-) and (π^-,π^+) reactions in ^{16}O and ^{40}Ca over a range of incident pion energies from 120 to 270 MeV [27,31]. More limited data have been obtained for ^{103}Rh and ^{208}Pb.

Extensive data have also been obtained more recently for inclusive DCX in the *s*- and *p*-shell nuclei: ^{3}He [32], ^{4}He [33,34], ^{6,7}Li, ^{9}Be [35], and ^{12}C. The results of these measurements will be reported elsewhere.

II. EXPERIMENTAL METHOD

For most of the kinematic range of the present experiment, detection of a pion of charge opposite to that of the incident pion provides an unambiguous signature of a double charge exchange reaction. The probability of successive single charge exchanges on separate nuclei is not competitive with that for a double charge exchange reaction within a single nucleus. The small contribution of pion-induced pion production [e.g., $(\pi^+,\pi^+\pi^-)$] in limited portions of phase space will be discussed later.

In this experiment pions of "opposite" charge were identified by a 180° double focusing magnetic spectrometer [36–38] equipped with multiwire proportional chambers, a plastic scintillator, and a threshold Cherenkov counter as shown in Fig. 2. Some properties of the spectrometer are given in Table I. This spectrometer, set for a charge opposite to that of the incident beam, is an extremely potent filter against other types of events, such as elastic, inelastic, and quasielastic pion scattering. The only undesirable particles found to traverse the spectrometer were electrons and positrons and, when set for positive charge, protons and other light ions. All of these particles could be clearly identified by the detection system. Because the spectrometer is double focusing, particles accepted into a relatively large phase space are

TABLE I. Properties of the spectrometer used in the DCX measurements.

Bending radius	60 cm
Solid angular acceptance	15 msr
Dispersion	2.3 cm/%
Momentum bite	9.5%
Maximum momentum	320 MeV/*c*
Target-to-detector flight path	3.6 m
Angular range	20°–135°
Resolution	$\delta p/p=1.7\times10^{-3}$ (intrinsic); determined in practice by the momentum width and spot size of the beam

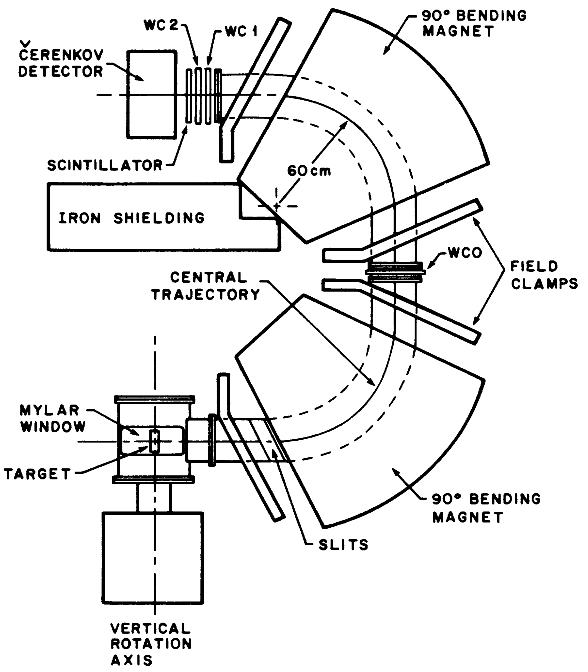

FIG. 2. Schematic drawing of the spectrometer used to detect the DCX pions. Position measurements in the multiwire proportional chambers labeled WC1 and WC2 determined the momentum of the outgoing pion, and particle identification was provided by the scintillator and Cherenkov detector, as discussed in the text. A valid event trigger required a fourfold coincidence of signals from WC0, WC1, WC2, and the scintillator; including the wire chamber WC0 in the trigger ensured that the detected particle traveled through the spectrometer.

brought to a focus on small, easily shielded detectors, minimizing the sensitivity to ambient background. 30 cm of steel below the detectors shielded them from the target and 15 cm of steel shielded the sides of the detectors. Cross sections of 200 $\text{nb}\,(\text{sr MeV}/c)^{-1}$ were routinely measured with adequate precision, and cross sections of one-tenth this size could easily have been observed given sufficient time. This spectrometer-detector system operated with no detectors in the vicinity of the intense incident pion beam required to measure these small cross sections with good statistical accuracy.

Detecting pions with kinetic energy as low as 10 MeV (54 MeV/c momentum) was a further critical requirement for adequate coverage of the phase space of the outgoing pions in double charge exchange, as will be evident in the data we present here. In many cases a significant fraction of the pion yield was found to lie at energies below 30 MeV. This spectrometer-detector system could efficiently detect pions at these low momenta because of the relatively short 3.6-m flight path, the almost continuous vacuum between target and focal plane, and the thin detectors. Corrections to the cross sections for pion decay are relatively small and will be discussed in Sec. III E 1.

The scattering chamber and spectrometer vacuum jacket are joined and hold a continuous vacuum from the target to the focal plane, except for a 30-mm air gap bounded by two 125-μm Mylar windows between the two 90° magnets where a multiwire proportional chamber is inserted. An active shunt bridging the second magnet reduces its field to compensate for the energy lost by pions in the midspectrometer vacuum windows and wire chamber. Beyond the focal plane, particles pass through a 250-μm aluminum window into the air and through the remaining detectors.

The system of detectors comprises the midspectrometer wire chamber, a pair of wire chambers immediately beyond the focal plane (which is inaccessible inside the vacuum chamber of the spectrometer), a thinly wrapped 1.6-mm-thick plastic scintillation detector, and a fluorocarbon (FC-88) Cherenkov detector. The wire chambers [39] have delay-line readouts of coordinates in two dimensions; both the anode and one of the cathode planes of each chamber are arrays of wires. A quadruple coincidence among the three wire chambers and the scintillator, timed by the scintillator, triggers the computer to record the pulse heights of signals from the scintillator and Cherenkov detector and the delay times of signals from the wire chambers. The midspectrometer wire chamber is included in the trigger to guarantee that a particle traverses the second bend and, hence, to eliminate triggers from the copious background of soft electrons in the vicinity of the focal plane. The timing information available from this chamber also distinguishes pions from very slow protons by establishing the particles' time of flight between the chamber and the scintillator.

The scattering chamber was equipped with a remotely movable and rotatable target ladder that allowed exposure of one of six targets to the beam. The targets, except for ^{16}O, were solid foils of natural Ca (96.9% ^{40}Ca), natural Rh (100% ^{103}Rh), and enriched Pb (98.7% ^{208}Pb). The ^{16}O target was liquid H_2O contained in a cell with walls of 50 μm Mylar. The thickness of this target was measured [27] to be 1.50 g cm^{-2} with the cell walls fully stretched under vacuum. The Ca, Rh, and Pb targets had thicknesses of 1.01, 0.94, and 0.57 g cm^{-2}, respectively.

The incident beam for these measurements was that of the high-energy pion (P^3) channel at LAMPF. Positive and negative pion beams over a wide range of energies with fluxes ranging from about 10^7 to above $10^9\ \text{s}^{-1}$ are available. For these experiments the beam was transported through the channel with a momentum acceptance of 2% (4% at low energies where the beam intensity is diminished) and brought to an achromatic focus at the target within a roughly circular spot 1 cm in diameter at the half intensity points of its profile. The steering and focus of the beam were observed continuously throughout the experiment with a multiwire beam profile monitor [40].

The beam intensity was monitored by two devices with complementary properties. The primary monitor was an argon-filled ionization chamber located about 1.2 m upstream of the target, and the secondary monitor was a simple measurement of pion reactions 2.3 m downstream of the target. Two scintillator telescopes, one on either side of the beam line, detected particles emerging at 90° from a 3.2-mm CH_2 target. The ionization chamber responded to all charged particles in the incident beam, and hence its calibration as a monitor of the pion flux depended on the fraction of contaminant particles in the beam. The downstream telescope monitor, which responded essentially only to pion reactions with the CH_2 target, could not be used for the primary measurement of the pion flux for two reasons: The flux incident upon the CH_2 target depended on the thickness of the target in place in the scattering chamber upstream, and at small spectrometer angles, the pion beam was intercepted by the iron of the spectrometer. However, this device did monitor the stability of the ion chamber response. An additional check was a measurement of the primary proton beam current with a toroid placed just upstream of the pion production target. Occasional corrections of a few percent based on the ratio of the signals from the two pion monitors were made to the double charge exchange cross sections.

Neither of the monitors provides an absolute measurement of the pion flux. Therefore the entire experimental arrangement, including the beam monitors, target location and orientation, spectrometer angular acceptance and momentum bite, and response of the detectors, was calibrated as a whole by observing elastic pion-proton scattering. The ladder in the scattering chamber also held a thin CH_2 target for this purpose, as well as a thin carbon target for background subtraction. Details of this procedure are discussed below.

III. DATA REDUCTION

A. Particle identification

In addition to the pions of interest, electrons, muons, protons, and other light ions reach the focal plane of the spectrometer. During measurements of (π^-,π^+) cross sections, the proton rate exceeded the pion rate by a factor of up to 100. For most of the momentum range observed in this experiment, the protons lose much more energy than do the pions in the scintillator and can readily be identified by their pulse heights alone. Figure 3 shows a pulse-height spectrum for 156-MeV/*c* particles where the large proton background is clearly separated from the pions which have kinetic energy 70 MeV. At lower momenta the protons only partially penetrate the scintillator, producing pulse heights comparable to those of the pions. However, in these cases the velocities of the particles are sufficiently different such that the time of flight between the midspectrometer wire chamber and the scintillator may be used to separate pions and protons. Figure 4 shows an isometric projection of events versus time of flight and scintillator pulse height for a case where the energy-loss information is ambiguous, viz., 143 MeV/*c* (60-MeV pions). The combination of energy loss and time of flight also identifies deuterons, tritons, and ^{3}He nuclei.

The baryons can be eliminated event by event. However, since pions above 180 MeV/*c* produce light in the Cherenkov counter, the pulse-height spectra corresponding to pions and electrons overlap to a degree dependent on the momentum of the particles. The number of pions in a sample of events was determined by analysis of these pulse-height spectra. Both the sum and product of the pulse heights from two phototubes, located above and below the fluorocarbon radiator, were examined. The product was found to be less strongly correlated with the vertical position of a particle's trajectory. The product spectrum was accumulated for each measurement at a given spectrometer momentum setting. This spectrum was then fitted with a linear combination of two functions, one representing the response of the detector to pions alone and the other to electrons alone, to determine the relative abundances of the two particles. The pion response functions for various momenta were determined from observations of elastic scattering on CH_2 and quasielastic scattering on C, in which the number of pions detected overwhelms the number of electrons. The electron response function, which is independent of momentum, was obtained from spectra at low-momentum settings where only electrons radiate Cherenkov light. For momenta up to ~60 MeV/*c*, the scintillator pulse height

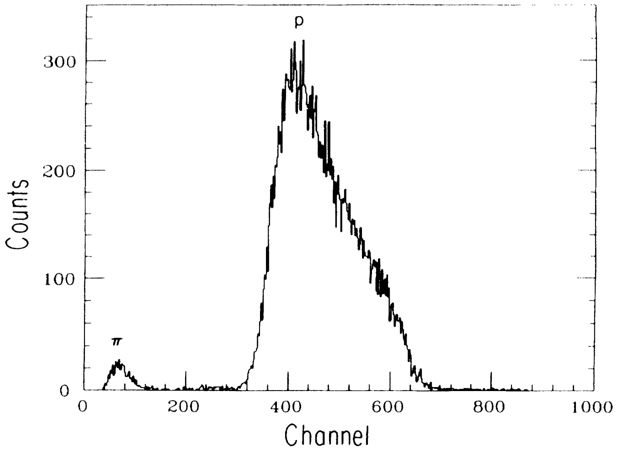

FIG. 3. Pulse-height spectrum from the scintillator (see Fig. 2) for a spectrometer momentum setting of 156 MeV/*c*, which corresponds to a pion kinetic energy of 70 MeV. The pions are seen to be clearly separated from protons and heavier charged particles.

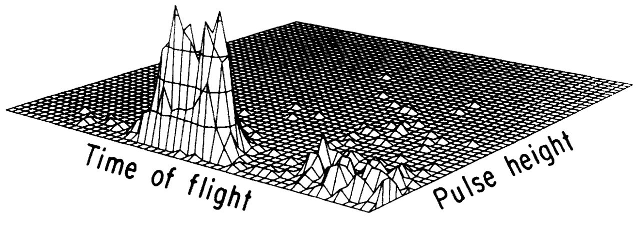

FIG. 4. Isometric projection illustrating the correlation of the pulse height in the scintillator with the particle's time of flight between WC0 and the scintillator for a spectrometer momentum setting of 143 MeV/*c*, which corresponds to a pion kinetic energy of 60 MeV. This information allows the separation of pions and positrons from protons. (The Cherenkov detector provides the necessary information for the separation of pions and positrons, as discussed in the text.)

also differentiates between electrons and pions. The electron-pion separation procedure is described in detail in Ref. [27].

No attempt is made to distinguish between muons and pions in the detection system. The spectrometer is double focusing and has a relatively small momentum acceptance, properties that allow muon contaminations to be determined reliably by Monte Carlo techniques, as will be discussed later.

B. Trajectory reconstruction

Measurements of the (x,y) coordinates in the two wire chambers, located at $z=15.9$ and 24.8 cm beyond the focal plane, determined the trajectory of each detected particle at the focal plane. This location establishes the momentum, and limits on the four-dimensional phase-space volume $x(dx/dz)y(dy/dz)$ restrict acceptable trajectories to those expected for particles originating from the target. This restriction reduces the contamination by particles scattering from the spectrometer vacuum chamber and by muons and electrons that come from pion decay inside the spectrometer.

C. Spectrometer and beam monitor calibration

The dispersion and momentum acceptance of the spectrometer were determined by observing elastic pion-proton scattering. With the incident pion beam adjusted for a momentum bite of 1%, the spectrometer field was varied in small steps to move the elastically scattered pions across the focal plane. This procedure simultaneously determined the dispersion and relative acceptance as a function of position along the dispersion direction of the focal plane. The acceptance function, shown in Fig. 5, has a momentum width $\Delta p/p_0=8\%$, full width at half maximum, with a "flat top" of 4%.

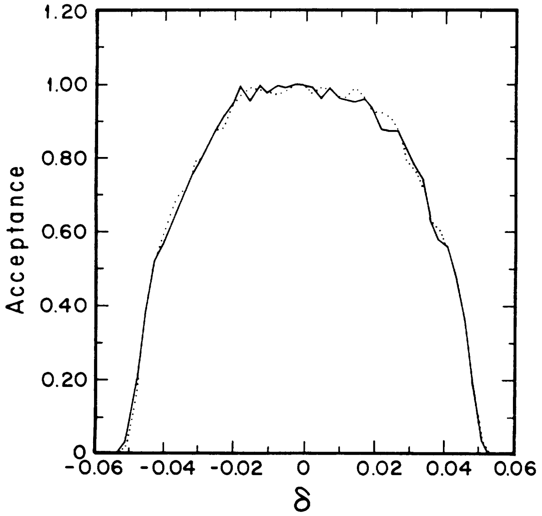

FIG. 5. Relative acceptance of the spectrometer plotted against $\delta=(p-p_0)/p_0$. The solid and dotted curves represent two measurements of the acceptance performed during the experiment.

The product of the ionization chamber calibration constant and the solid angular acceptance of the spectrometer was determined from the cross section for elastic pion-proton scattering. For each incident energy and charge of pions used in the measurement of DCX cross sections, the elastically scattered pions from the CH_2 target, and the corresponding background from the C target, were observed at six to eight angles in 10° or 20° steps. Measuring a complete angular distribution both improves the statistics of the calibration and reveals any angular dependence in the acceptance of the spectrometer. To obtain the normalization constant, values of the π-p cross sections were interpolated to energies and angles of interest with an energy-dependent phase shift analysis [37,41] which reproduces benchmark measurements [42] in the relevant energy range to 1% or 2%.

D. Determination of the doubly differential cross section

Data from each magnetic field setting of the spectrometer were generally used to derive one measurement of the doubly differential cross section at the outgoing pion energy corresponding to the central momentum. This procedure is valid if the cross section as a function of momentum does not have a strong curvature over the momentum or angular acceptance of the spectrometer. At high energies, where the cross section does exhibit a strong curvature over a full momentum bite, the focal plane was divided into two or three segments, yielding measurements of the cross section at two or three momenta and making the effects of the curvature negligible. The cross section may be written as

$$\frac{d^2\sigma}{d\Omega\, dE}=\frac{N_\pi}{\Delta E\, N_i \Delta\Omega\, x} ,$$

where N_π is the number of pions that would have been detected in the absence of pion decay, N_i is the number of pions incident on the target, $\Delta\Omega$ is the spectrometer solid angle, and x is the target thickness. The factor ΔE is the mean energy acceptance of the portion of the focal plane used. The product of the number of pions in the incident beam and solid angular acceptance of the spectrometer $(N_i\Delta\Omega)$ is directly obtained by multiplying the digitized representation of the total charge produced in the ionization chamber by the normalization factor determined from elastic scattering. A number of factors that must be considered in relating the measured events to N_π are considered in Sec. III E.

E. Corrections

1. Pion decay

To relate the actual number of events observed to N_π, the detected number must be divided by the "survival fraction." This correction, which accounts for pion decay, also properly includes the effect of muons that are counted as pions by the detection apparatus. At the lowest momentum of observation, more than two-thirds of the pions decay in the 3.6-m flight path. However, some of the muons from pion decay still reach the detectors, which cannot distinguish between pions and muons that fall within the specified phase space. These muons can be divided into two classes: those arising from pion decay in the spectrometer and those from decay in the scattering chamber. The former must originate from pions within the momentum and scattering angle acceptance of the spectrometer, whereas the latter may originate from pions of very different momenta and traveling in different directions from pions detected at the focal plane. All the pion decay and muon contamination effects are summarized as a single momentum-dependent survival fraction

$$F(p_\pi)=f_d+f_s(1-f_d)+f_c \; .$$

The first term, the pion decay survival fraction, is simply $f_d=\exp(-m_\pi L/p_0 c\tau)$, where the spectrometer length L is 365 cm, p_0 is the spectrometer central momentum, and $c\tau=780$ cm. A fraction f_s of the muons arising from the fraction $(1-f_d)$ of pions that decay in the spectrometer will still reach the focal plane and satisfy the phase-space and particle identification constraints. This momentum-dependent fraction is estimated by simulating the spectrometer optics and phase-space constraints with the code DECAY TURTLE [43]. It results in a correction to the measured cross sections of typically 3%.

A sometimes more significant effect of pion decay occurs in the scattering chamber and in the drift space before the first dipole. The additional flux from these "cloud muons" is estimated with a Monte Carlo calculation that simulates the geometry of the scattering chamber. This simulation assumes as input a momentum distribution of inclusive DCX pions at a desired beam energy; these pions are allowed to decay in the scattering chamber. Applying the phase-space acceptance of the spectrometer as determined from DECAY TURTLE, the distribution of muons from these pions can be obtained. The correction f_c is then given as the ratio of the number of muons detected at a given momentum divided by the number of pions that would have been detected in the absence of pion decay. This correction, which was found to be relatively insensitive to the input momentum distribution, resulted in a 20% increase in the cross section for the lowest outgoing pion energies. At 30 MeV the correction is less than 10% and it becomes less than 1% at the highest outgoing energies. Further details are given in Ref. [27].

2. *Multiple scattering and energy loss in* WCO

The spectrometer provides a continuous path in vacuum for scattered particles between the target and focal plane with the exception of a wire chamber (WC0) and the associated vacuum windows located after the first 90° bend. Multiple scattering in this material broadens the angular divergence of transported particles and thus reduces the number of particles that satisfy the focal-plane phase-space constraints. In addition, low-energy pions will suffer a non-negligible energy loss in the wire chamber and windows. Accordingly, for pions of energy less than 30 MeV, the magnetic field in the second dipole was reduced to compensate for the energy lost. This reduced field gives a smaller absolute momentum acceptance for the second dipole, further reducing the yield at the focal plane. A single correction for these two effects was obtained by a calculation similar to that for the muon contamination using DECAY TURTLE, assuming the energy loss and multiple scattering to arise from 49.3 $\text{mg}\,\text{cm}^{-2}$ $(1.41\times10^{-3}$ radiation lengths) of Mylar. The ratio of the results without and with the "Mylar" in place is the factor by which the focal-plane yields must be multiplied to obtain corrected cross sections. The correction was calculated at several outgoing pion energies and fitted by the form $[1+A\exp(-Bp)]$, where p is the pion momentum, $A=43.3$, and $B=0.084$ $(\text{MeV}/c)^{-1}$. For 10-MeV outgoing pions, a correction of 47% was applied; at 30 MeV, the correction was only 2%.

3. *Differential energy loss*

Scattered pions lose several MeV in the targets; below 100 MeV, the energy loss becomes strongly energy dependent. This effect not only necessitates a correction to the measured pion energy, but because the energy spread of a group of particles becomes larger in passing through the material, also reduces the number of pions falling into a fixed spectrometer energy acceptance. As the cross sections presented here are differential in E, they must be multiplied by a factor $(dE_{\text{in}}/dE_{\text{out}})$, where E_{in} and E_{out} are the energies before and after the pions traverse the target. To calculate this derivative analytically, the momentum loss dp/dx in the neighborhood of a given central momentum of the spectrometer was parametrized as $dp/dx=Ap^\gamma$. Integrating this expression through a target of thickness x yields

$$p_{\text{out}}=[p_{\text{in}}^{1-\gamma}+(1-\gamma)Ax]^{1/(1-\gamma)} ,$$

from which it follows that

$$\frac{dE_{\text{in}}}{dE_{\text{out}}}=\frac{E_{\text{out}}}{p_{\text{out}}}\frac{p_{\text{in}}}{E_{\text{in}}}\{p_{\text{in}}^{1-\gamma}/[p_{\text{in}}^{1-\gamma}+(1-\gamma)Ax]\}^{\gamma/(1-\gamma)} .$$

This correction assumes that all the pions traverse the same thickness of target material. Since DCX pions are produced uniformly throughout the target, this correction should be averaged over the range of possible thicknesses. The result of this averaging is not significantly different from that obtained by using an equivalent thickness equal to half the actual target thickness. The correction may be further refined by averaging over the momentum acceptance function of the spectrometer. The case in which the largest correction must be applied is that in which 10-MeV pions are detected from the H_2O target when its normal is 40° to the spectrometer direction, where the effective target thickness is 2 cm. Here the cross sections must be multiplied by 2.35 and the data point assigned an outgoing pion energy of 15 MeV. With this target configuration, the correction factor at 30 MeV is 1.22; for all other target angles and materials, the correction is smaller.

4. *Attenuation of incident and scattered particles in the target*

In addition to causing energy loss, thick targets also absorb and rescatter the DCX pions. A correction for absorption, obtained from known cross sections, is straightforward. However, pions lost from one part of the spectrum by rescattering can reappear at a lower pion energy, distorting the measured spectrum in a manner which depends on the shape of the undistorted spectrum. In general, a proper correction would involve a Monte Carlo simulation with the quasielastic and DCX spectra for each beam energy and target as input. We shall argue that such an approach is unnecessary.

The major pion-nucleus reaction channels are elastic scattering, inelastic scattering, absorption, and single charge exchange. Elastic scattering can be ignored since it produces very little change in the pion energy and is forward peaked. There is thus little distortion in the DCX spectrum or angular distribution due to this process occurring either before or after the DCX reaction. Furthermore, because inclusive DCX is found to be fairly isotropic, even large-angle elastic scattering should not appreciably affect the spectra. Absorption and single charge exchange will attenuate the pion flux both before and after DCX.

The bulk of inelastic scattering is quasielastic, with outgoing pions of around half the incident energy. Such reactions will remove flux from part of the DCX spectrum, but may add flux to a lower energy part of the spectrum. As seen in the present data, the doubly differential cross section for DCX is usually larger at lower energies. Thus the relative increase in a low-energy part of the spectrum will be smaller than the relative decrease in the higher-energy part of the spectrum from which the rescattered pions originated. If a pion undergoes an inelastic scattering and then DCX, the DCX reaction will be taking place at an energy lower than the incident beam energy. Because DCX total cross sections are seen to increase monotonically with energy, DCX reactions after inelastic scattering will add less to the spectrum than was removed. Therefore inelastic scattering will also be treated as if it were absorption.

The effect of rescattering in the target can now be estimated using the sum of the cross sections for all channels except elastic scattering. This sum $\sigma_{\text{att}}(E)=\sigma_{\text{tot}}(E)-\sigma_{\text{elastic}}(E)$ must be evaluated for the incident beam energy and for each outgoing pion energy. An attenuation factor may be derived by assuming that the pion traverses half the target before undergoing DCX. To correct the cross sections, the yield must be divided by

$$1-[\sigma_{\text{att}}(E_{\text{in}})+\sigma_{\text{att}}(E_{\text{out}})]N_0 x/(2A)\ ,$$

where N_0 is Avogadro's number, x is the target thickness, and A is the atomic mass of the target. The cross sections are obtained by interpolating experimental results tabulated by Ashery *et al.* [44]. The corrections thus derived are always less than 6%.

5. *Target frame background*

DCX data were taken with an empty target frame and, for comparison with the ^{16}O measurements, an empty H_2O target cell. The pion yields from the empty frame and empty H_2O cell were approximately 1% and 10%, respectively, of the full-target yields. Therefore these yields were observed at more widely spaced spectrometer settings. To derive an interpolation function for these data, each target-out spectrum was fitted by the product of a first-order polynomial and a function representing the distribution of DCX events derived from the volume of phase space available to a four-body final state. As will be seen, this latter function approximately reproduces the observed shape of the DCX pion spectra. The fitted curves were subtracted from the corresponding target-in spectra to yield the final doubly differential cross sections.

6. *Background reactions*

Electron-, photon-, and pion-induced pion production processes can yield "DCX-like" events. Electrons in the incident beam interact in the target, and photons from the decay of π^0's (resulting from single charge exchange) interact both in the target and with the spectrometer material to produce pions. Photoproduction and electroproduction processes were estimated to contribute less than 1% to the DCX yields and were thus ignored.

At sufficiently high incident energies, pion-induced pion production can contribute to the observed yield of low-energy pions because the experiment did not distinguish between DCX events with one pion in the final state and production events with two or more pions. For the reaction (π^-,π^+) on ^{16}O, pion-induced pion production on the hydrogen in the water target contributed to the apparent DCX yield. At 240 MeV the integrated cross section for the $\pi^-+p\rightarrow\pi^++\pi^-+n$ reaction [36,45] is about 100 μb, which increased the apparent DCX yield by 3.5%. At lower energies this background reaction becomes insignificant (the threshold energy is 172 MeV). A correction for this background was applied to the integrated DCX cross sections, but not to the doubly differential cross sections or the angular distributions.

Pion production in nuclei has only recently been studied experimentally. At TRIUMF, Grion *et al.* [46] observed the $^{16}\text{O}(\pi^+,\pi^+\pi^-)$ process at incident energy 280 MeV and obtained an energy- and angle-integrated cross section of 2250±350 μb. At PSI, Rahav *et al.* [47] observed the isospin-symmetric reaction $(\pi^-,\pi^-\pi^+)$ on ^{12}C at 292 MeV and obtained an integrated cross section of 978±109 μb. If one assumes that the $(\pi,2\pi)$ cross section in nuclei has the same energy dependence as that for the $p(\pi^-,\pi^-\pi^+)n$ process [36,45] and that it scales approximately with an effective number of nucleons (N_{eff}), [44] then one can estimate from these measurements the contribution of the $(\pi,2\pi)$ process to the DCX cross sections measured in the present experiment. Unfortunately, the TRIUMF and PSI results are not mutually consistent. For example, for ^{16}O at 270 MeV, one deduces a $(\pi,2\pi)$ cross section of 1.69±0.26 mb from the measurement of Grion *et al.* [46] and 0.64±0.07 mb from that of Rahav *et al.* [47,48]. If one simply takes the free-nucleon cross section [36] and multiplies it by N_{eff}, one obtains [27] 1.1 mb. These cross sections may be compared with the corresponding measured DCX cross section of 5.9±0.5 mb. We shall comment further on the $(\pi,2\pi)$ process when the DCX results are compared with theoretical calculations in Sec. V, but we emphasize here that pion production contributes little to the yields at incident energies below 240 MeV.

The "^{40}Ca" target was in fact natural Ca. The 3% abundance of neutron-rich isotopes in this target was estimated [27] to produce only a 1% difference in the $^{40}\mathrm{Ca}(\pi^+,\pi^-)$ cross sections. This correction was ignored.

F. Derivation of angular distributions

The doubly differential cross sections obtained at each angle were integrated over outgoing pion energy to derive singly differential cross sections, or angular distributions, $d\sigma/d\Omega$. To carry out the integration, each spectrum was fitted by least squares with the function

$$(a_0+a_1E+\cdots+a_nE^n)P(E) .$$

The quantity $P(E)$ represents the distribution of events derived from four-body phase space, where the four bodies are the pion, two nucleons, and the residual nucleus. The polynomial provided sufficient flexibility to allow a good fit to the data, and the phase-space distribution enforced a cutoff of the function at zero energy and at the kinematic limit for inclusive DCX. A fourth-order polynomial adequately described most of the data. The fitted function was integrated numerically over energy E to yield $d\sigma/d\Omega$. The relative statistical error in $d\sigma/d\Omega$ was estimated by dividing the result by $\sqrt{N}$, where N is the total number of counts accumulated in the entire spectrum. This statistical error was increased by adding a 2% error in quadrature to account for possible long-term fluctuations in the normalization. An additional systematic uncertainty arises from constraining the fitting function to be zero at zero pion energy, whereas the measured spectra are consistent with different extrapolations to zero energy. This uncertainty was taken as one-half of the area under the fitted function between zero and the energy of the lowest-energy data point.

G. Derivation of total reaction cross sections

The differential cross sections were integrated over angle to obtain the total DCX cross sections. Although no measurements were made at angles less than 25° or greater than 130°, only 23% of the total solid angle lies in these regions. Moreover, the measured angular distributions were found to be smoothly and generally very slowly varying with angle. Accordingly, the angular distributions were fitted by a series of Legendre polynomials,

$$\frac{d\sigma(\theta)}{d\Omega}=\sum_{i=0}^{n} a_i P_i(\cos\theta) ,$$

where the number of terms was one less than the number of measurements of $d\sigma/d\Omega$. Varying n between 1 and this value was found to produce less than a 1% change in the total cross section. The total cross section is then given by

$$\sigma=4\pi a_0 .$$

The relative statistical error in the integrated cross section was taken as equal to the statistical error in the 80° differential cross section, multiplied by $(\chi^2)^{1/2}$ if this quantity, resulting from the Legendre polynomial fit, was greater than 1. The statistical error in the normalization to elastic scattering, estimated to be 3%, was added in quadrature.

H. Systematic errors

The major systematic uncertainties are those in the corrections applied to the data which have been discussed in Sec. III E, corrections which were sizable at low outgoing pion energies. The uncertainty in the pion decay correction was derived by assuming a 0.25-m uncertainty in the spectrometer length. The uncertainties in the energy-loss and multiple-scattering corrections were estimated to be one-half of the correction applied. Since the correction for attenuation of pions in the target is relatively small, its uncertainty was ignored. An uncertainty in the electron-pion separation at low outgoing pion energies was also included. The combined effect of these uncertainties on two spectra, one at incident energy 120 MeV and one at 240 MeV, was evaluated. For each outgoing pion energy, the relative uncertainties in all the corrections were added in quadrature. Spectra with the resulting uncertainty added and subtracted were created; these two "worst case" spectra were fitted by polynomial-times-phase-space functions as described above. The area between these functions is taken as the overall systematic error due to the corrections and was found to be ±15% at 120 MeV and ±7.5% at 240 MeV. The systematic error due to the extrapolation of the spectra to zero energy was added in quadrature to the above error to give an overall energy-dependent systematic uncertainty of 18% at 120 MeV and 9% at 240 MeV. It is assumed that this error is the same for all targets and scattering angles at a given incident energy. Errors for other incident energies were estimated by interpolating between these values. Uncertainties in the target thicknesses were typically 3–4% for the DCX targets and 2% for the CH_2 target used in the elastic-scattering normalization.

IV. RESULTS

Doubly differential cross sections for inclusive DCX have been measured over a broad range of experimental parameters. For both ^{16}O and ^{40}Ca, the reaction $A(\pi^+,\pi^-)X$ was observed at incident pion energies of 120, 150, 180, 210, 240, and 270 MeV. The $A(\pi^-,\pi^+)X$

reaction was observed in both nuclei at 180, 210, and 240 MeV. For each reaction, spectra were typically measured at three scattering angles (25°, 80°, and 130°), although five angles (25°, 50°, 80°, 105°, and 130°) were observed for positive pions at 180, 210, and 240 MeV. For ^{103}Rh and ^{208}Pb, data were obtained at three angles with positive and negative pions at 180 and 240 MeV. At each incident energy and angle, cross sections were measured at 10–15 outgoing pion energies from 10 MeV to the kinematic limit of the DCX continuum.

The measured doubly differential cross sections for inclusive DCX are shown in Figs. 6, 7 (^{16}O), 8, 9 (^{40}Ca), 10, 11 (^{103}Rh), 12, and 13 (^{208}Pb). For reference, the spectra are compared to the distribution of events derived from four-body phase space. For example, in Fig. 6 the curves represent the phase-space distribution for the reaction $\pi^+ + {}^{16}\text{O} \rightarrow \pi^- + {}^{14}\text{O} + p + p$. For a given incident energy, the phase-space distributions have the same normalization for all angles, obtained by matching the curve to the measured cross section at outgoing energy 50 MeV at the smallest angle observed.

One sees that for ^{16}O (Figs. 6 and 7) at low incident pion energies and small angles, the spectra resemble the phase-space distributions quite closely. At higher incident pion energies and/or larger angles, a systematic deviation appears: The spectra exhibit an excess of low-energy pions and a deficiency of high-energy pions. At 210 and 240 MeV, there appears to be a slight excess of high-energy pions at forward angles, a feature to which we shall return later. Comparison of Fig. 7 with Fig. 6 shows the (π^-,π^+) spectra to be very similar in shape and magnitude to those for (π^+,π^-).

For ^{40}Ca (Figs. 8 and 9), the same qualitative trends are seen. However, the deviations of the spectra from the

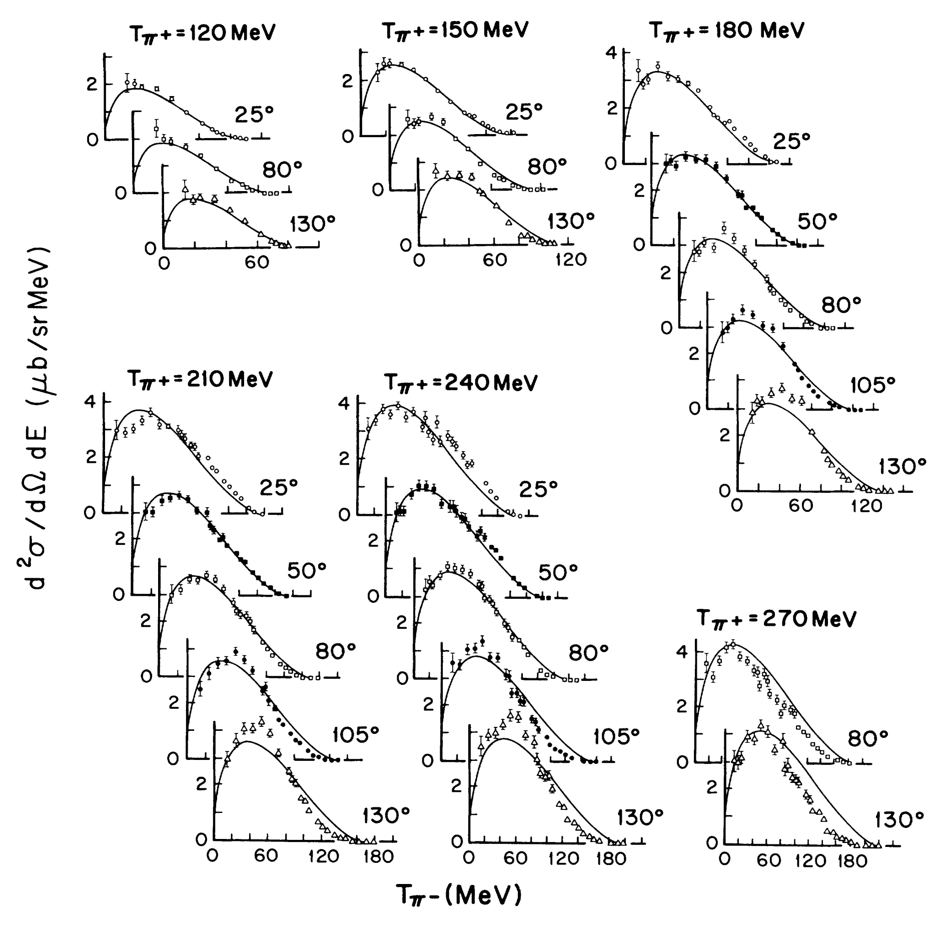

FIG. 6. Doubly differential cross section $d^2\sigma/d\Omega\, dE$ for the reaction ^{16}O(π^+,π^-) at incident energies 120, 150, 180, 210, 240, and 270 MeV. At 180, 210, and 240 MeV, the spectrum of outgoing pions was measured at a series of angles, 25°, 50°, 80°, 105°, and 130°; fewer angles were observed at the lowest and highest energies. The error bars indicate statistical uncertainties only. The curves represent the distribution of DCX events derived from the volume of phase space available to a four-body final state. The curves have been normalized to the data at outgoing energy $T_{\pi^-} = 50$ MeV at the most forward angle observed.

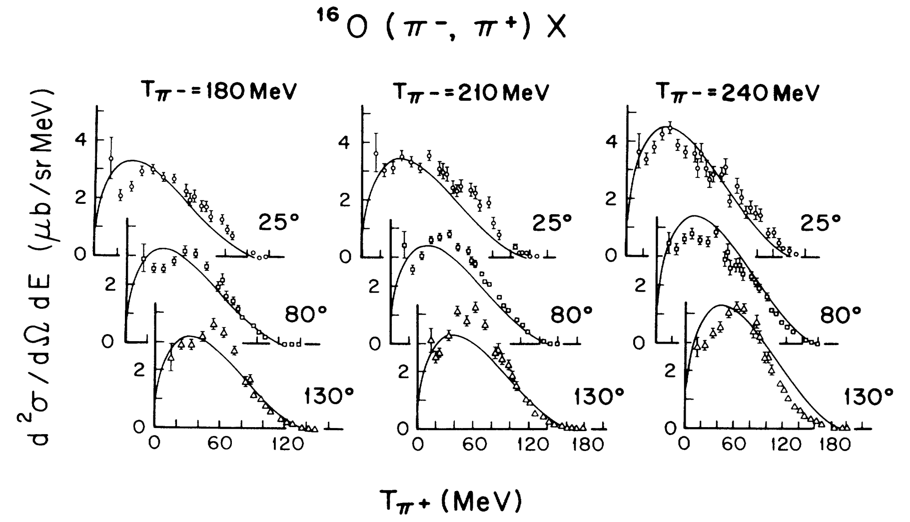

FIG. 7. Doubly differential cross section $d^2\sigma/d\Omega\, dE$ for the reaction ^{16}O(π^-,π^+) at incident energies 180, 210, and 240 MeV and outgoing pion angles 25°, 80°, and 130°. The error bars indicate statistical uncertainties only. The curves are as in Fig. 6.

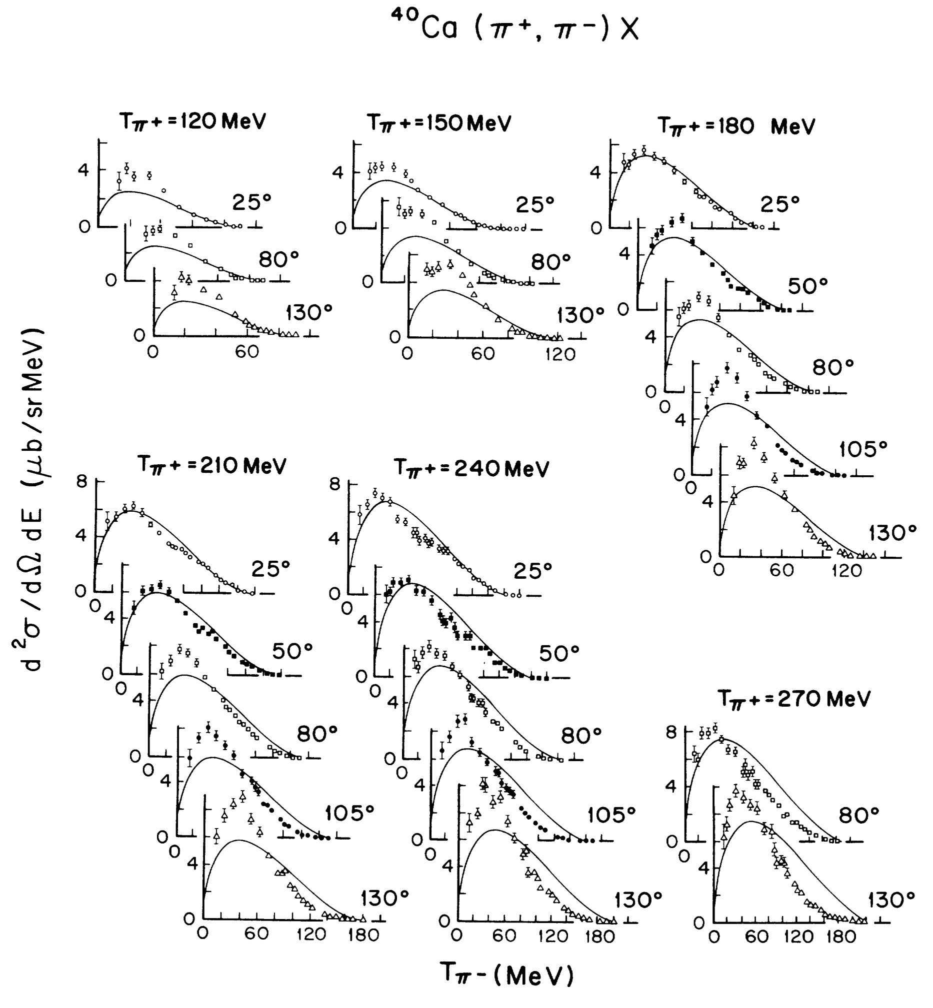

FIG. 8. As Fig. 6 for the reaction ^{40}Ca(π^+,π^-).

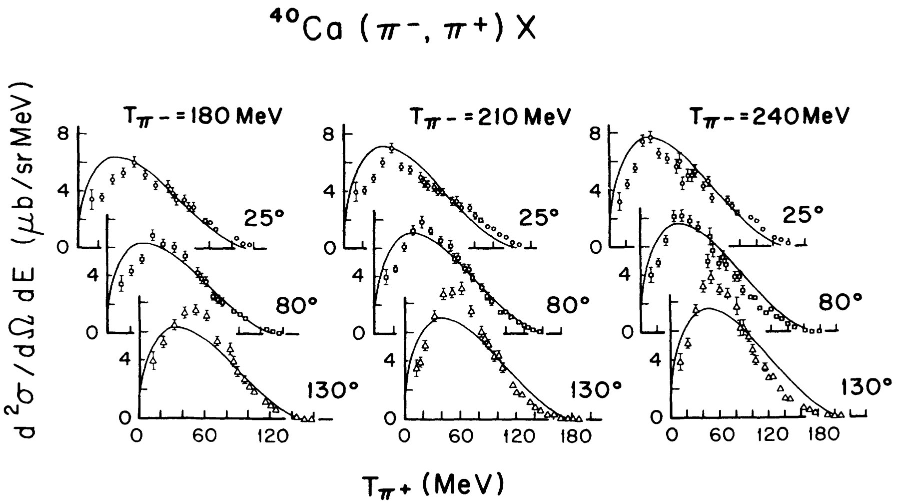

FIG. 9. As Fig. 7 for the reaction ^{40}Ca(π^-,π^+).

phase-space distributions (excess at low energy, deficiency at high energy) occur at lower incident energy and smaller angles. The doubly differential cross sections for the heavy nuclei ^{103}Rh and ^{208}Pb (Figs. 10–13), which were measured only at $E_{\text{inc}} = 180$ and 240 MeV, bear very little resemblance to four-body phase space at any angle. Moreover, the (π^+,π^-) and (π^-,π^+) spectra have very different shapes. This difference in shape is consistent with one's expectation from the Coulomb attraction (repulsion) of the negative (positive) pions. The (π^+,π^-) and (π^-,π^+) cross sections also have substantially different magnitudes. In these neutron-rich nuclei, one would expect the (π^+,π^-) cross section to exceed that for (π^-,π^+), but perhaps not by as large an amount as observed. We shall return to this point at the end of this section. The dashed curves shown at 130° are the results of a theoretical calculation [49] which will be discussed later.

Figures 14–17 show the angular distributions of the (π^+,π^-) and (π^-,π^+) reactions. The angular distributions for ^{16}O are somewhat forward peaked, those for ^{40}Ca nearly isotropic, and those for ^{103}Rh and ^{208}Pb backward peaked. The backward peaking for heavy nuclei might be a manifestation of the strong interaction of the

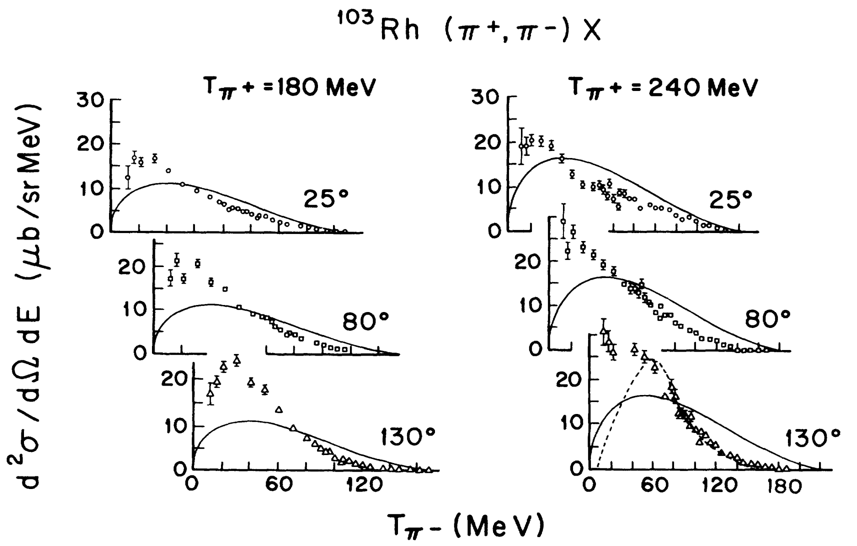

FIG. 10. Doubly differential cross section $d^2\sigma/d\Omega\, dE$ for the reaction ^{103}Rh(π^+,π^-) at incident energies 180 and 240 MeV and outgoing pion angles 25°, 80°, and 130°. The error bars indicate statistical uncertainties only. The solid curves are as in Fig. 6. The dashed curve shown at 240 MeV and 130° represents the result of a theoretical calculation [49] as discussed in Sec. V.

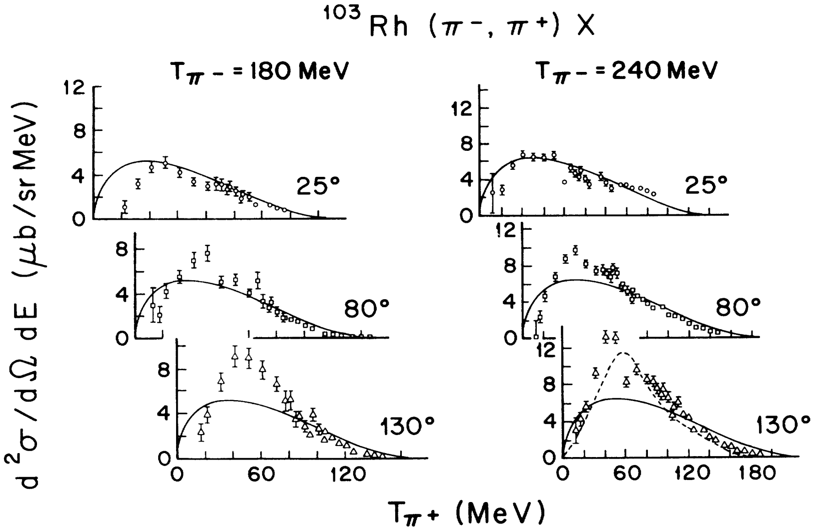

FIG. 11. As Fig. 10 for the reaction ^{103}Rh(π^-,π^+).

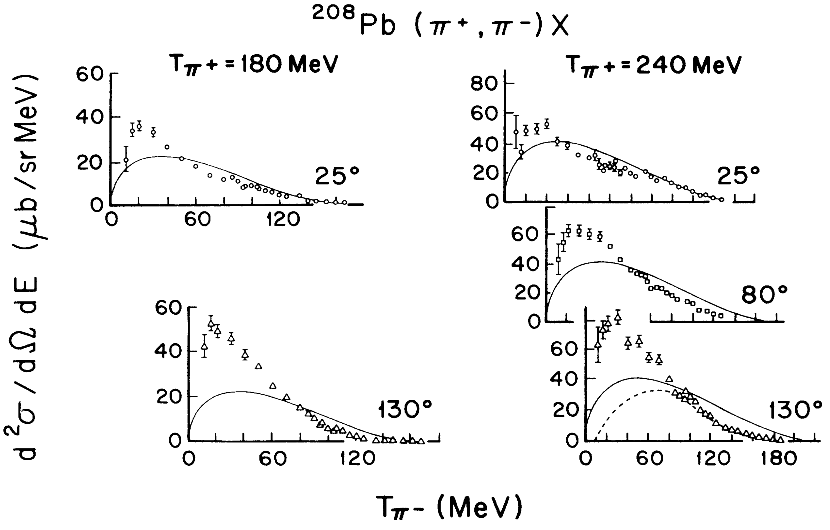

FIG. 12. As Fig. 10 for the reaction ^{208}Pb(π^+,π^-).

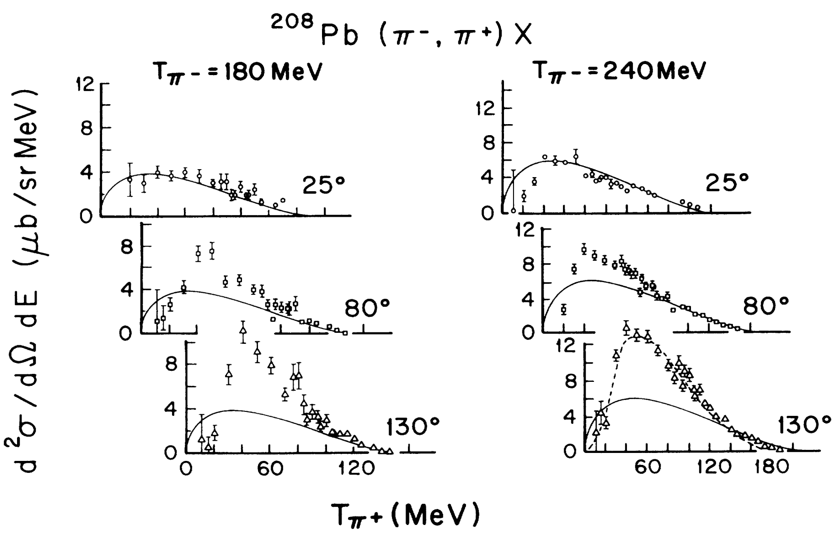

FIG. 13. As Fig. 10 for the reaction ^{208}Pb(π^-,π^+).

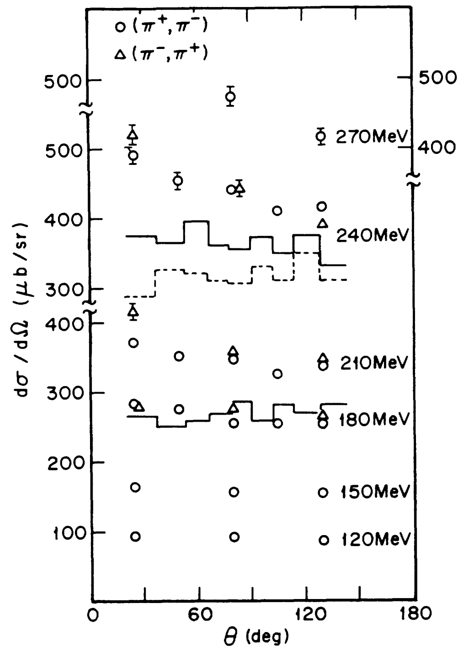

FIG. 14. Angular distributions $d\sigma/d\Omega$ for the reactions $^{16}O(\pi^+,\pi^-)$ (circles) and $^{16}O(\pi^-,\pi^+)$ (triangles). Only the statistical errors are shown. There is an additional systematic uncertainty which varies smoothly with incident energy from 17% at 120 MeV to 8% at 270 MeV. The histograms represent the results of a theoretical calculation [30] at incident energies 180 and 240 MeV (see Sec. V).

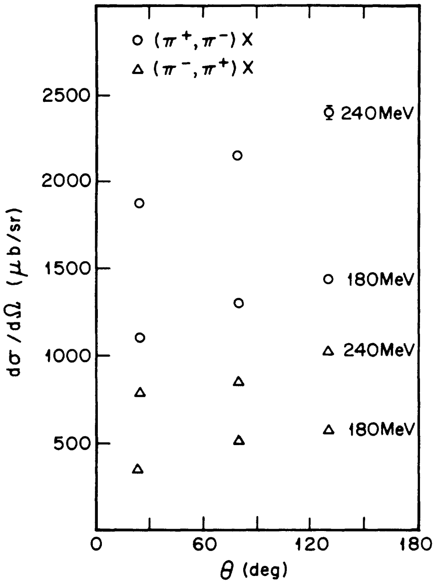

FIG. 16. Angular distributions $d\sigma/d\Omega$ for the reactions $^{103}Rh(\pi^+,\pi^-)$ (circles) and $^{103}Rh(\pi^-,\pi^+)$ (triangles) at 180 and 240 MeV. Only the statistical errors are shown. There is an additional systematic uncertainty of 12% at 180 MeV and 8% at 240 MeV.

pions: They will interact primarily in the "rear" surface of the nucleus, that illuminated by the incident beam, from which they have a much larger probability of escaping into the backward hemisphere than into the forward hemisphere. The histograms shown in Figs. 14 and 15 represent theoretical predictions for DCX in ^{16}O and ^{40}Ca at incident energies 180 and 240 MeV [30].

Table II lists the total reaction (angle-integrated) cross sections for the (π^+,π^-) and (π^-,π^+) processes as a function of the incident pion energy. The (π^+,π^-) cross sections for ^{16}O and ^{40}Ca are plotted in Fig. 18 and are

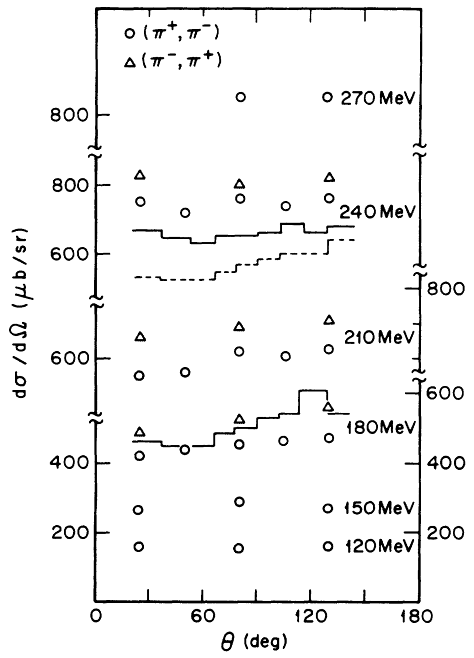

FIG. 15. As Fig. 14 for the reactions $^{40}Ca(\pi^+,\pi^-)$ and $^{40}Ca(\pi^-,\pi^+)$.

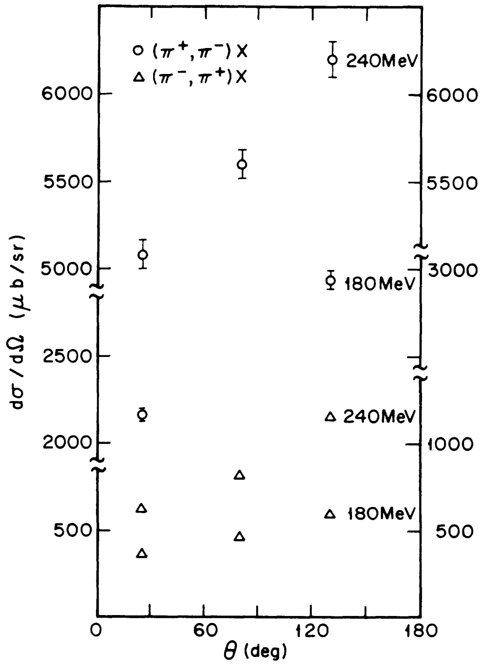

FIG. 17. As Fig. 16 for the reactions $^{208}Pb(\pi^+,\pi^-)$ and $^{208}Pb(\pi^-,\pi^+)$.

TABLE II. Total reaction cross section for inclusive double charge exchange.

		σ (mb)			
T_{inc} (MeV)		^{16}O	^{40}Ca	^{103}Rh	^{208}Pb
120	(π^+,π^-)	1.14±0.22	1.99±0.37		
150	(π^+,π^-)	2.00±0.31	3.51±0.56		
180	(π^+,π^-)	3.30±0.44	5.72±0.74	16.4±2.1	30.8±6.8
	(π^-,π^+)	3.43±0.46	6.69±0.85	6.25±1.21	6.14±0.76
210	(π^+,π^-)	4.33±0.59	7.52±0.86		
	(π^-,π^+)	4.51±0.56	8.68±0.95		
240	(π^+,π^-)	5.47±0.54	9.38±0.90	27.5±2.6	72.0±6.5
	(π^-,π^+)	5.32±0.54	10.22±0.95	11.33±1.01	11.53±1.09
270	(π^+,π^-)	5.86±0.50	10.64±0.86		

seen to rise monotonically with energy. This behavior is in marked contrast to that of other inclusive pion cross sections (e.g., inelastic scattering and absorption) [44] which tend to decrease or level off above the Δ(1232) resonance energy. However, one must recall that DCX is a two-step (at least) process. An incident pion of above-resonance energy can lose considerable energy in its first interaction so that it is "on resonance," with a large cross section, in its second interaction.

The energy dependence of the DCX and other pion interaction cross sections has been treated in a classical calculation using the Boltzmann equation by Hüfner and Thies [26]. Their prediction for the ^{12}C(π^+,π^-) cross section has been multiplied by $(\frac{16}{12})^{2/3}$ for comparison with our results for ^{16}O and is shown as the solid curve in Fig. 18. Although continuing to rise above the Δ(1232) resonance, the theoretical cross section does not reproduce the observed energy dependence and underpredicts the measurement by a large factor for $E_{\text{inc}} \geq 200$ MeV. The short- and long-dashed curves represent theoretical predictions of Vicente *et al.* [30], which will be discussed later.

Figure 19 shows the integrated cross sections for $E_{\text{inc}} = 180$ and 240 MeV, plotted as a function of nuclear mass A. The (π^+,π^-) and (π^-,π^+) cross sections are seen to behave quite differently; whereas the former increase monotonically with A, the latter appear to "saturate" at $A=40$, so that the (π^-,π^+) cross section for Pb is about equal to that for Ca, despite the fact that Pb has 4 times as many protons as Ca. It is possible that the (π^-,π^+) cross sections for heavy nuclei are suppressed by a "screening" effect: The large number of excess neutrons, with which negative pions of resonance energies

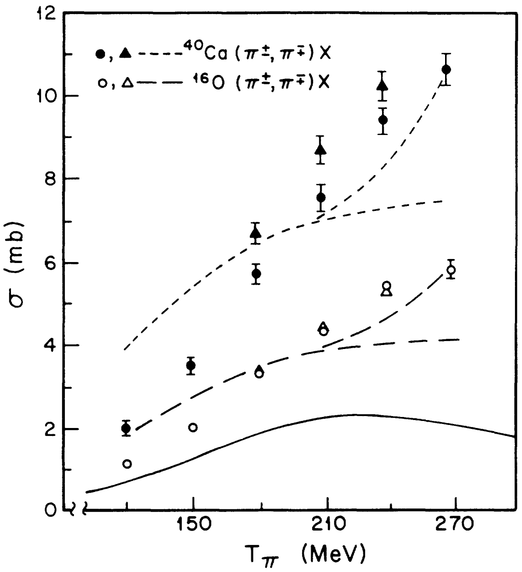

FIG. 18. Total reaction cross sections vs E_{inc} for DCX in ^{16}O (open symbols) and ^{40}Ca (solid symbols) as a function of incident energy. As in Figs. 14–17, the circles represent (π^+,π^-) cross sections and the triangles (π^-,π^+) cross sections. Only the statistical errors are shown. The systematic uncertainty varies smoothly with incident energy from 17% at 120 MeV to 8% at 270 MeV, for all four sets of data. The solid curve is the result of a classical calculation by Hüfner and Thies [26], as discussed in the text. The long- and short-dashed curves are the predictions of a cascade-model calculation of Vicente *et al.* [30] for DCX in ^{16}O and ^{40}Ca, respectively. The upper branch of each curve represents the inclusion of pion-induced pion production.

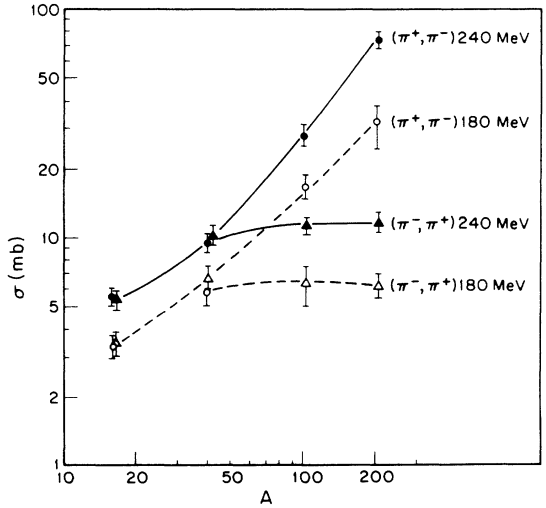

FIG. 19. Total DCX reaction cross sections vs nuclear mass number A at incident energy 180 and 240 MeV. The error bars shown include both statistical and systematic uncertainties. The curves are drawn to guide the eye.

prefer to interact, effectively removes the π^-'s before they can charge exchange with the protons. Since there are no heavy proton-rich nuclei, this effect is not seen in the (π^+,π^-) cross sections. A simple classical model, based on DCX proceeding via two sequential single charge exchanges in competition with other, more probable reactions, provides a good representation of the A dependence of both the (π^+,π^-) and (π^-,π^+) cross sections [50].

V. COMPARISON WITH CALCULATIONS

Theoretical analysis of inclusive DCX, or indeed of other pion-induced reactions in which particles are ejected from the nucleus, has proved to be complicated. Certain qualitative features of the mechanisms active in this reaction may be brought out by examining a sequence of increasingly complex calculations.

The simplest calculation [27] assumes that DCX takes place via two sequential single charge exchange (SCX) reactions on free nucleons in a degenerate Fermi gas ($|\mathbf{k}| \le k_F = 250$ MeV/c). Requiring that the recoil nucleons each have $k > k_F$ enforces Pauli blocking. The SCX cross sections are assumed to be identical to those for this process on a free proton. The results of this calculation are compared with the ^{16}O(π^+,π^-) data at $E_{\rm inc} = 240$ MeV, with arbitrary normalization, in Fig. 20. The shapes of the calculated spectra (represented by the light solid curves) clearly do not correspond at all well to those measured. Nonetheless, examining some features of this model proves interesting. The double-peaked structure seen at forward angles, of which perhaps a hint is seen in the data for ^{16}O and ^{40}Ca, is found to be a consequence of the nonisotropic $(1+3\cos^2\theta)$ angular dependence of the free-nucleon SCX cross section. This angular dependence, which arises from the p-wave nature of the pion-nucleon interaction at Δ-resonance energies, favors sequences of SCX reactions in which a DCX pion appears at a forward angle by means either of two small-angle SCX's (with small energy loss) or two large-angle SCX's (with large energy loss). If one employs an isotropic SCX cross section in the calculation, the double peaking disappears, as illustrated by the dashed curves in Fig. 20.

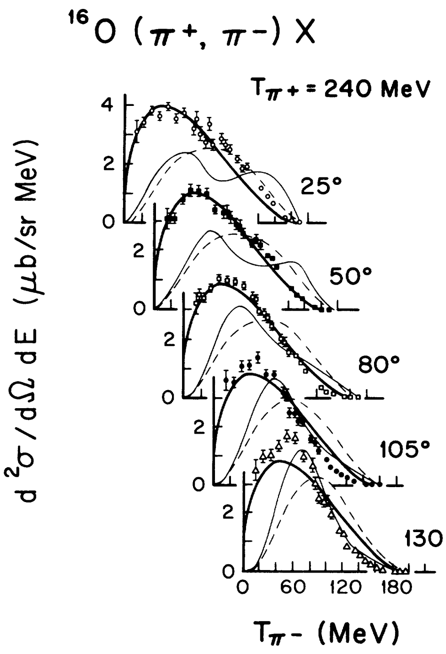

FIG. 20. Comparison of the doubly differential cross section $d^2\sigma/d\Omega\,dE$ for the reaction ^{16}O(π^+,π^-) at 240 MeV with the prediction of a model [27] in which the incident pion undergoes two single charge exchanges with nucleons in a degenerate Fermi gas (light solid curves). Replacing the $1+3\cos^2\theta$ angular dependence of the free single charge exchange cross section with an isotropic cross section results in the dashed curves. The heavy solid curves represent the four-body phase-space distribution as in Fig. 6. The normalization of the curves is arbitrary.

Double-peaked spectra have in fact been observed at forward angles in DCX on very light nuclei [1,32–34]. One might hypothesize that sequential SCX is indeed the dominant DCX reaction mechanism and that more complex processes (e.g., triple scattering) become increasingly important as the number of nucleons in the target increases, thus obscuring this signature of the elementary double-scattering process. This hypothesis is consistent with the location of the average measured strength in the spectra shown in Fig. 20 at a lower energy than that calculated, suggesting that more than two interactions are generally occurring in DCX.

A more realistic picture that includes this effect is provided by an intranuclear cascade model [27], in which the pion is not limited to two interactions and the competing processes of absorption and inelastic scattering without charge exchange are also allowed to occur. The pion is followed through the nucleus until it either escapes or is absorbed. The nucleon density distribution is assumed to be spherically symmetric and is represented by a three-parameter Fermi function. As in the two-step Fermi-gas model calculation, the nucleon momentum distribution is assumed to be uniform within the sphere $|\mathbf{k}| \le k_F = 250$ MeV/c, the free pion-nucleon cross sections are used, averaged over nucleon momenta, and Pauli blocking of the recoil nucleon is included. Since pion absorption cannot occur on a free nucleon, this cross section, in particular its dependence on pion energy and nuclear density, must be obtained from a model. Two models [26,51] of absorption have been employed. In both of them the absorption cross sections vary as the square of the nuclear density, but the two treatments have very different energy dependences [52]. Perhaps surprisingly, the choice of absorption model has little influence on the cross sections resulting from the cascade calculation. Predictions for inelastic scattering, absorption, single and double charge exchange in ^{16}O and ^{40}Ca were all found [27] to be insensitive to the choice of absorption model. The prediction of the doubly differential cross sections shown in Fig. 21 used the model of Hüfner and Thies [26]. Spectra obtained using the Beder-Bendix model [51] are essentially indistinguishable from these [27]. The cascade calculations, represented by the smooth curves, are compared with the ^{16}O(π^+,π^-) data at three incident energies. Comparing the results with those of the two-step calcula-

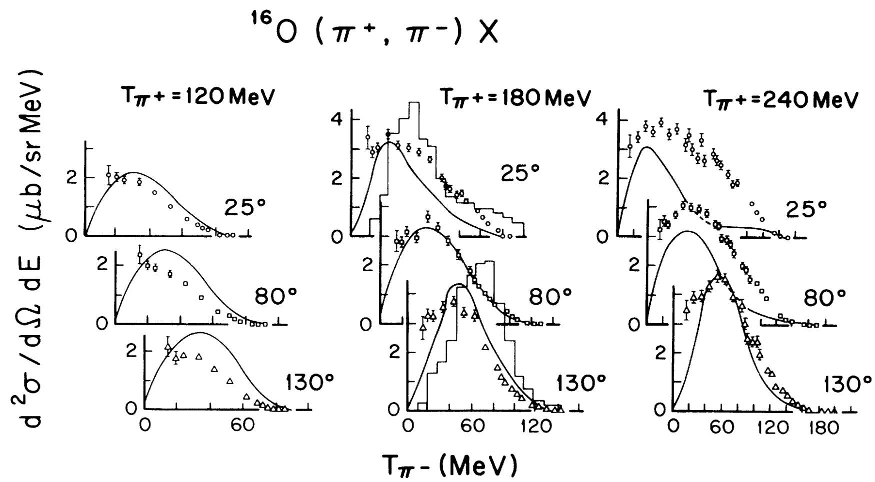

FIG. 21. Comparison of the doubly differential cross sections $d^2\sigma/d\Omega\, dE$ for the reaction ^{16}O(π^+,π^-) at 120, 180, and 240 MeV with the predictions of two intranuclear cascade models as discussed in the text. The solid curves are the results of the calculation of Ref. [27], and the histograms at 180 MeV are taken from Ref. [30].

tion shown in Fig. 20, one sees spectra in Fig. 21 that do peak at lower outgoing pion energies. The agreement with the data is fairly good at incident energy 180 MeV. However, the calculation underestimates the measurement at forward angles for high outgoing energies. This effect becomes much more pronounced at 240 MeV, where the cascade cross section is too low at all angles forward of 130°. This underestimate could be due to either the effective scattering cross sections in the nuclear medium being too large (yielding too large a probability for multiple scattering and thus shifting too much strength down to lower pion energies) or the absorption cross section being too large at high energies, depleting the DCX cross section. The former effect could accentuate the latter: Multiple scattering will cause high-energy pions to lose energy and to appear in the resonance region where they have a larger probability of being absorbed. Evidence of these effects is seen in the calculated [27] total cross section for inelastic scattering, which is smaller than the data [53] at 240 MeV, and in the absorption cross section, which is too large [44,54]. Moreover, since the probability of multiple interactions will depend on the amount of nuclear matter the pion has to traverse, an overestimate of these interactions will produce the largest disagreement with the data at forward angles, as is seen in Fig. 21, and also produce angular distributions that are more backward peaked than those measured, as is also seen in Fig. 21.

The above comparisons indicate that a more detailed microscopic treatment is required to produce quantitative agreement with the DCX data. One obvious defect of these simple, classical calculations [27] is the approximate treatment of the effects of the nuclear medium on the πN interaction. A more complete treatment would include the correlation between the nuclear density and the nucleon momentum and binding energy. Oset and co-workers [28–30] evaluate the intrinsic probabilities for pion inelastic scattering, single charge exchange, and absorption by calculating the imaginary part of the pion-nucleus optical potential as a function of the nuclear density. In the framework of the Δ-hole model, the *p*-wave pion-nucleus optical potential in infinite nuclear matter is expanded in terms of one-particle–one-hole (1p1h), 2p2h, and 3p3h excitations. Probabilities for the various reactions are related to different sources of the imaginary part of the optical potential; these probabilities are applied to reactions in finite nuclei by means of the local density approximation, corrected to account for the finite range of the interactions. Oset and co-workers [28–30] also calculated the *s*-wave contribution to the πN interaction, since pions can reach the low energies at which this amplitude is important through multiple collisions. The effect of neglecting the real part of the pion-nucleus optical potential (i.e., the elastic-scattering channel) was investigated and found to be very small for $T_\pi \geq 140$ MeV. Double charge exchange in this model occurs via two sequential single charge exchanges, as in Fig. 1(a). Meson-exchange mechanisms such as that in Fig. 1(b) are not included.

In their calculations of the inclusive DCX cross sections, Vicente *et al.* [30] included pion-induced pion production [e.g., $(\pi^+,\pi^+\pi^-)$], using a model previously developed by Oset and Vicente [55]. They found that the cross section for this process increases rapidly with incident pion energy, from about 15% of the DCX cross section at 240 MeV to one-third to one-half of the DCX cross section at 270 MeV. This prediction, 1.96 mb for ^{16}O at $E_{\rm inc}=270$ MeV, is consistent with the experimental result of Grion *et al.* [46], but exceeds that of Rahav *et al.* [47] by about a factor of 3.

Some of these theoretical results are compared with the present data in Figs. 10–15, 18, and 21. We first examine the doubly differential cross sections. The calculations for DCX in ^{16}O at 180 MeV, where there is no contribution from pion production, are shown as the histograms in Fig. 21. The agreement with the data is not very good. Vicente *et al.* [30] comment that the semiclassical methods used in their calculation are not suitable for outgoing pion energies below 100 MeV and that at higher energies one could expect better agreement. Indeed, at $E_{\rm inc}=270$ MeV the calculation provides a rather good representation of the data for both ^{16}O and ^{40}Ca at 130°, as seen in Figs. 7 and 8 of Ref. [30]. The comparison of experiment and theory at 80° (see the same two figures), however, shows poor agreement: The inclusion of pion production causes the theory to exceed the data at low outgoing pion energies, suggesting that this effect has been overestimated. At high outgoing energies where this process cannot occur, the theory seriously underpredicts the measured cross section, suggesting that the DCX part of the cross section is not correctly modeled.

More recently, the calculations of doubly differential cross sections have been extended to other nuclei [49]. Predictions at 130° and 240 MeV incident energy for (π^+,π^-) and (π^-,π^+) in ^{103}Rh and ^{208}Pb are shown as the dashed curves in Figs. 10–13. The agreement with the measured (π^-,π^+) cross sections (Figs. 11 and 13) is fairly good, whereas it is quite poor for (π^+,π^-) (Figs. 10 and 12). This is not understood by the authors of Ref. [49], who speculate that the effect might arise from different proton and neutron density distributions.

Figures 14 and 15 exhibit the calculated angular distributions [30] for DCX in ^{16}O and ^{40}Ca, respectively, at 180 and 240 MeV; at the higher energy, predictions with (solid histograms) and without (dashed histograms) inclusion of pion-induced pion production are shown. The calculation does not distinguish between (π^+,π^-) and (π^-,π^+) reactions. The agreement at 180 MeV with the ^{16}O data is fairly good. It is not clear how to evaluate the prediction for ^{40}Ca, as the measured (π^+,π^-) and (π^-,π^+) cross sections differ. At 240 MeV, even with the inclusion of pion production, which may well be unrealistically large in this model, both the ^{16}O and ^{40}Ca cross sections are significantly underpredicted. The calculation does not account for the forward peaking of the angular distribution observed in the ^{16}O data.

Figure 18 shows the predicted energy dependence of the total reaction cross sections for DCX in ^{16}O (long-dashed curves) and ^{40}Ca (short-dashed curves), with and without the inclusion of pion production. The calculation does not reproduce the observed energy dependence for either nucleus; the discrepancy is worse for ^{40}Ca than for ^{16}O. Inclusion of production does allow the theoretical cross sections to agree with those measured at 270 MeV. However, as mentioned previously, the present data for the doubly differential cross sections at this incident energy, which the calculation exceeds in the region of the spectrum in which pion production is kinematically allowed, as well as the $(\pi,2\pi)$ measurements of Rahav *et al.* [47,48], indicate that this effect may have been overestimated by the authors of Ref. [30].

The detailed comparison of these theoretical predictions with the experimental results that has been presented here makes it clear that further work is necessary. The calculation must be extended to account properly for the propagation of lower-energy pions if one is to make a serious quantitative comparison of its results with the data. The deficiencies in the calculation of the outgoing DCX pion spectrum, in which the strength lies predominantly below 100 MeV even for 270-MeV incident pions, undermines the claim that a large $(\pi,2\pi)$ component is substantiated by the results of this experiment. The effect of the Coulomb interaction, which has not been included in the transition operator, should be investigated. Also, it would be interesting to see the result of extending the model beyond the assumptions of the local density approximation to a more sophisticated derivative expansion, since much of the dynamics takes place at the nuclear surface. At present, it is difficult to judge at what nuclear size the approximation of using corrected infinite nuclei matter probabilities in finite nuclei should break down.

VI. SUMMARY AND CONCLUSIONS

An extensive set of doubly differential cross sections for the inclusive (π^+,π^-) and (π^-,π^+) reactions has been measured for nuclei of mass between $A=16$ and 208 and for incident pion energies in the $\Delta(1232)$ resonance region. The systematic behaviors of the doubly differential, singly differential, and total reaction cross sections have been examined in terms of the phenomenology of the DCX process. A semiclassical calculation based on a simple sequential model of two single charge exchange reactions on nucleons in a Fermi gas fails to reproduce the shape of the observed pion spectra. An intranuclear cascade calculation is somewhat more successful in accounting for the shapes of the spectra, but does not predict the measured dependence on angle or incident energy. A more microscopic theory which obtains the DCX cross sections simultaneously with those for other inclusive pion-nucleus reaction channels constitutes a promising beginning, but fails to reproduce in detail the measured doubly differential, singly differential, and total reaction cross sections for DCX in ^{16}O and ^{40}Ca. The present data should stimulate further theoretical work. Quantitative understanding of this process, in which double scattering is the leading term, should be extremely valuable in advancing our knowledge of the multiple interactions of pions in nuclei.

Tabulations of the doubly differential cross sections reported here are deposited with the Physics Auxiliary Publication Service [56].

ACKNOWLEDGMENTS

The participation of D. A. Clark, S. Høibråten, D. W. MacArthur, P. Mansky, E. Piasetzky, C. R. Schermer, T. Soos, and H.-J. Ziock in various stages of the experimental measurements is gratefully acknowledged. This work was supported in part by the U.S. Department of Energy. One of us (G. A. R.) wishes to acknowledge the financial support of Associated Western Universities, Inc.

[1] J. Sperinde, D. Fredrickson, V. Perez-Mendez, and B. Smith, Phys. Lett. **32B**, 185 (1970); J. Sperinde, D. Fredrickson, and V. Perez-Mendez, Nucl. Phys. **B78**, 345 (1974).

[2] R. E. P. Davis, A. Beretvas, N. E. Booth, C. Dolnick, R. J. Esterling, R. E. Hill, M. Raymond, and D. Sherden, Bull. Am. Phys. Soc. **9**, 127 (1964).

[3] L. Gilly, M. Jean, R. Meunier, M. Spighel, J. P. Stroot, and P. Duteil, Phys. Lett. **19**, 335 (1965).

[4] L. Kaufman, B. W. Gauld, V. Perez-Mendez, J. M. Sperinde, and S. H. Williams, Phys. Lett. **25B**, 536 (1967); L. Kaufman, V. Perez-Mendez, and J. Sperinde, Phys. Rev. **175**, 1358 (1968).

[5] J. E. Ungar, R. D. McKeown, D. F. Geesaman, R. J. Holt, J. R. Specht, K. E. Stephenson, B. Zeidman, and C. L. Morris, Phys. Lett. **144B**, 333 (1984); T. P. Gorringe *et al.*, Phys. Rev. C **40**, 2390 (1989).

[6] Yu. A. Batusov, S. A. Bunyatov, V. M. Sidorov, and V. A. Yarba, Yad. Fiz. 3, 309 (1966) [Sov. J. Nucl. Phys. **3**, 223 (1966)]; Yu. A. Batusov, S. A. Bunyatov, V. M. Sidorov, V. A. Yarba, G. Ionice, E. Losnianu, and V. Mihul, *ibid.* [**5**, 249 (1967)]; Yu. A. Batusov, S. A. Bunyatov, V. M. Sidorov, and V. A. Yarba, *ibid.* [**6**, 727 (1968)]; Yu. A. Batusov, S. A. Bunyatov, N. Dalkhazhav, G. Ionice, E. Losneanu, V. Mihul, V. M. Sidorov, D. Tuvdendorzh, and V. A. Yarba, *ibid.* [**9**, 221 (1969)].

[7] L. Gilly, M. Jean, R. Meunier, M. Spighel, J. P. Stroot, P. Duteil, and A. Rode, Phys. Lett. **11**, 244 (1964).

[8] R. E. Mischke, A. Blomberg, P. A. M. Gram, J. Jansen, J. Zichy, J. Bolger, E. Boschitz, C. H. Q. Ingram, and G. Pröbstle, Phys. Rev. Lett. **44**, 1197 (1980).

[9] A. C. Phillips, Phys. Lett. **33B**, 260 (1970).

[10] R. I. Dzhibuti and R. Ya. Kezerashvili, Yad. Fiz. **39**, 419 (1984) [Sov. J. Nucl. Phys. **39**, 264 (1984)].

[11] R. I. Jibuti and R. Ya. Kezerashvili, Nucl. Phys. **A437**, 687 (1985).

[12] R. I. Dzhibuti and R. Ya. Kezerashvili, Fiz. Elem. Chastits At. Yadra **16**, 1173 (1985) [Sov. J. Part. Nucl. **16**, 519 (1985)].

[13] R. Ya. Kezerashvili, Yad. Fiz. **44**, 842 (1986) [Sov. J. Nucl. Phys. **44**, 542 (1986)].

[14] F. Becker and C. Schmit, Nucl. Phys. **B18**, 607 (1970).

[15] J.-F. Germond and C. Wilkin, Lett. Nuovo Cimento **13**, 605 (1975).

[16] R. I. Dzhibuti, R. Ya. Kezerashvili, and K. I. Sigua, Yad. Fiz. **32**, 1536 (1980) [Sov. J. Nucl. Phys. **32**, 795 (1980)].

[17] R. I. Jibuti, R. Ya. Kezerashvili, and K. I. Sigua, Phys. Lett. **102B**, 381 (1981).

[18] W. R. Gibbs, B. F. Gibson, A. T. Hess, and G. J. Stephenson, Phys. Rev. C **15**, 1384 (1977).

[19] J.-B. Jeanneret, M. Bogdanski, and E. Jeannet, Nucl. Phys. **A350**, 345 (1980).

[20] N. Carayannopoulos, J. Head, N. Kwak, J. Manweiler, and R. Stump, Phys. Rev. Lett. **20**, 1215 (1968).

[21] I. V. Falomkin, M. M. Kulyukin, V. I. Lyashenko, G. B. Pontecorvo, Yu. A. Shcherbakov, C. Georgescu, A. Mihul, F. Nichitiu, A. Sararu, and G. Piragino, Nuovo Cimento A **22**, 333 (1974); I. V. Falomkin, *et al.*, Lett. Nuovo Cimento **16**, 525 (1976).

[22] F. Gaille, S. Mureramanzi, M. Bogdanski, J.-B. Jeanneret, E. Jeannet, and D. Perrin, Nuovo Cimento A **40**, 31 (1977).

[23] A. Stetz *et al.*, Phys. Rev. Lett. **47**, 782 (1981); A. Stetz *et al.*, Nucl. Phys. **A457**, 669 (1986).

[24] R. I. Dzhibuti and R. Ya. Kezerashvili, Yad. Fiz. **34**, 1464 (1981) [Sov. J. Nucl. Phys. **34**, 810 (1981)].

[25] Yu. A. Batusov, V. I. Kochkin, and V. M. Mal'tsev, Yad. Fiz. **6**, 158 (1967) [Sov. J. Nucl. Phys. **6**, 116 (1968)].

[26] J. Hüfner and M. Thies, Phys. Rev. C **20**, 273 (1979).

[27] S. A. Wood, Los Alamos National Laboratory Report No. LA-9932-T, 1983.

[28] E. Oset, L. L. Salcedo, and D. Strottman, Phys. Lett. **165B**, 13 (1985).

[29] L. L. Salcedo, E. Oset, M. J. Vicente-Vacas, and C. Garcia-Recio, Nucl. Phys. **A484**, 557 (1988).

[30] M. J. Vicente, E. Oset, L. L. Salcedo, and C. Garcia-Recio, Phys. Rev. C **39**, 209 (1989).

[31] S. A. Wood, J. L. Matthews, G. A. Rebka, Jr., P. A. M. Gram, H. J. Ziock, and D. A. Clark, Phys. Rev. Lett. **54**, 635 (1985).

[32] M. Y.-D. Wang, S. B. thesis, Massachusetts Institute of Technology, 1987; J. J. Vail, S. M. thesis, Massachusetts Institute of Technology, 1989.

[33] E. R. Kinney, J. L. Matthews, P. A. M. Gram, D. W. MacArthur, E. Piasetzky, G. A. Rebka, Jr., and D. A. Roberts, Phys. Rev. Lett. **57**, 3152 (1986).

[34] E. R. Kinney, Los Alamos National Laboratory Report No. LA-11417-T, 1988.

[35] P. Mansky, S. B. thesis, Massachusetts Institute of Technology, 1986.

[36] D. M. Manley, Los Alamos National Laboratory Report No. LA-9101-T, 1981.

[37] J. B. Walter, Los Alamos National Laboratory Report No. LA-8377-T, 1979.

[38] A. T. Oyer, Los Alamos National Laboratory Report No. LA-6599-T, 1976.

[39] C. L. Morris, H. A. Thiessen, and G. W. Hoffmann, IEEE Trans. Nucl. Sci. **NS-25**, 141 (1978).

[40] G. J. Krausse and P. A. M. Gram, Nucl. Instrum. Methods **156**, 365 (1978).

[41] J. B. Walter and G. A. Rebka, Jr., Los Alamos National Laboratory Report No. LA-7731-MS, 1979.

[42] J. R. Carter, D. V. Bugg, and A. A. Carter, Nucl. Phys. **B58**, 378 (1973).

[43] K. L. Brown and Ch. Iselin, "DECAY TURTLE (Trace Unlimited Rays Through Lumped Elements), A Computer Program for Simulating Charged Particle Beam Transport Systems, including Decay Calculations," CERN Report No. 74-2, 1974.

[44] D. Ashery, I. Navon, G. Azuelos, H. K. Walter, H. J. Pfeiffer, and F. W. Schlepütz, Phys. C **23**, 2173 (1981).

[45] C. W. Bjork *et al.*, Phys. Rev. Lett. **44**, 62 (1980).

[46] N. Grion *et al.*, Nucl. Phys. **492**, 509 (1989).

[47] A. Rahav *et al.*, Phys. Rev. Lett. **66**, 1279 (1991).

[48] Rahav *et al.* [47] speculate that the discrepancy may arise from the methods used to extrapolate the data for integration over 4π sr. Rahav *et al.* point out that the fraction of phase space covered in their work is 43 times larger than that covered in the experiment of Grion *et al.* [46].

[49] M. Vicente-Vacas and E. Oset, in *Pion-Nucleus Double Charge Exchange*, edited by W. R. Gibbs and M. J. Leitch (World Scientific, Singapore, 1990), p. 120.

[50] P. A. M. Gram, S. A. Wood, E. R. Kinney, S. Høibråten, P. Mansky, J. L. Matthews, T. Soos, G. A. Rebka, Jr., and D. A. Roberts, Phys. Rev. Lett. **62**, 1837 (1989).

[51] D. S. Beder and P. Bendix, Nucl. Phys. **B26**, 597 (1971).

[52] The inverse mean free path for absorption in the Hüfner-Thies model [26], calculated [27] as a function of incident

pion energy, shows a pronounced resonance peak, whereas that in the Beder-Bendix model [51] simply decreases monotonically with energy.

[53] C. H. Q. Ingram, P. A. M. Gram, J. Jansen, R. E. Mischke, J. Zichy, J. Bolger, E. T. Boschitz, G. Pröbstle, and J. Arvieux, Phys. Rev. C **27**, 1578 (1983).

[54] The calculations for ^{16}O were compared with the data for ^{12}C under the assumption that the cross section varies as $A^{2/3}$.

[55] E. Oset and M. J. Vicente, Nucl. Phys. **A454**, 637 (1986).

[56] See AIP document no. PAPS PRVCA-46-1903-25 for 25 pages of tabulations of the doubly differential cross sections reported here. Order by PAPS number and journal reference from American Institute of Physics, Physics Auxiliary Publication Service, 335 East 45th Street, New York, NY 10017. The prepaid price is $1.50 for a microfiche, or $5.00 for a photocopy. Airmail additional.